

Application of reactive transport modelling to growth and transport of microorganisms in the capillary fringe

P. Hron¹, D. Jost², P. Bastian¹, C. Gallert³, J. Winter², O. Ippisch^{1,4}

¹University of Heidelberg, Interdisciplinary Center for Scientific Computing, Im Neuenheimer Feld 368, 69120 Heidelberg, Germany

²Karlsruhe Institute of Technologie, Institut für Ingenieurbiologie und Biotechnologie des Abwassers, Am Fasanengarten Geb. 50.31, 76131 Karlsruhe, Germany

³University of Applied Science Hochschule Emden/Leer, Faculty of Technology, Microbiology – Biotechnology, Constantiaplatz 4, 26723 Emden, Germany

⁴Clausthal University of Technology, Department of Mathematics, Erzstraße 1, 38678 Clausthal-Zellerfeld, Germany
Email: pavel.hron@iwr.uni-heidelberg.de

Abstract

A multicomponent multiphase reactive transport simulator has been developed to facilitate the investigation of a large variety of phenomena in porous media including component transport, diffusion, microbiological growth and decay, cell attachment and detachment and phase exchange. The coupled problem is solved using operator splitting. This approach allows a flexible adaptation of the solution strategy to the concrete problem.

Moreover, the individual submodels were optimised to be able to describe behaviour of *Escherichia coli* (HB101 K12 pGLO) in the capillary fringe in the presence or absence of dissolved organic carbon and oxygen under steady-state and flow conditions. Steady-state and flow through experiments in a Hele-Shaw cell, filled with quartz sand, were conducted to study eutrophic bacterial growth and transport in both saturated and unsaturated porous media. As *E. coli* cells can form the green fluorescent protein (GFP), the cell densities, calculated by evaluation of measured fluorescence intensities (in situ detection) were compared with the cell densities computed by numerical simulation. The comparison showed the laboratory experiments can be well described by our mathematical model.

1 Introduction

There is a considerable ongoing effort aimed at understanding the microbial growth and transport in porous media [1, 2, 3, 4]. Microbial activity is of significant interest in various environmental applications such as *in situ* bioremediation [5], biodegradation of pollutants [6], dispersal of pathogenic microorganisms [7], protection of drinking water supplies, and for subsurface geochemistry in general.

The design of bioremediation schemes requires understanding the processes governing the growth, fate, cell attachment to solid surfaces and transport of the microbes under the particular physical, biological, and hydrogeological conditions involved [8]. The appropriate processes can be influenced e.g. by properties of the porous medium, the cells and pore water and gas composition [9, 10].

The soil microbial population can be affected by the availability of electron acceptors [11], nutrients [12] and bio-available water [13, 14]. The capillary fringe (CF), defined - in a wider sense than usual - as the region of the subsurface above the groundwater table, but still dominated by capillary rise, is a region where all these factors are abundantly available and it offers attractive growth conditions for aerobic and facultative anaerobic soil microorganisms [15, 16, 17]. It is thus a region where high microbial activity is to be expected. In the presence of dissolved molecular oxygen, most anaero-

bic metabolism is suppressed and aerobic bacteria are the dominant groups in aerated soils. In regions heavily contaminated with organic compounds the oxygen can be expected to be quickly depleted, so that aerobic metabolism will no longer dominate [18].

Reactive transport modelling is an essential tool for understanding microbial growth and transport in the subsurface [19] and has a significant impact e.g. on the treatment of contaminant retardation, bioremediation or intrinsic biodegradation in the subsurface, the description of nutrient fluxes and pollution distribution and on the experimental design in general. Many studies are often performed in laboratory scale experiments to identify the principal processes that affect microbial transport and appropriately designed mathematical models are developed and applied to predict the retention and transport of microorganisms in natural conditions [1, 20, 21].

Many researchers have studied the behaviour of microorganisms in porous media under saturated flowing conditions [22, 23, 24], but the transport in unsaturated porous media is more complicated [25, 26, 27, 28]. The purpose of this study is to develop a mathematical model describing multicomponent reactive transport processes in saturated and unsaturated porous media (especially in the CF) at the Darcy scale, to identify, quantify and investigate the relative importance of processes on microbiological growth and transport of *Escherichia coli*, to characterise the processes by appreciable microbial dynamics and to compare numerical simulations with laboratory experiments.

E. coli, an indicator bacterium for faecal pollution of the environment [4], can be used as a good example to investigate bacterial growth and transport in partially saturated porous media because *E. coli* cells may grow under aerobic and anaerobic conditions [29, 30]. In addition, *E. coli* is easy to detect and quantify, and the net negative surface charge and low inactivation rates ensure that they may travel long distances in the subsurface [31]. These characteristics make them a useful indicator of contamination of drinking water supplies or as indicator bacterium of faecal pollution of the environment [4] and is therefore a frequent research objective of many scientists [32, 33, 26, 34].

2 Model development

We assume that an unsaturated, incompressible porous medium under investigation consists of three phases $\mathcal{P} = \{s, l, g\}$: solid phase s and two fluids l, g , liquid and gas, respectively as in [35]. Each of these phases $\alpha \in \mathcal{P}$ is composed of a set of components \mathcal{K}_α .

Each phase α has its own mass phase density ρ_α and volume fraction θ_α . From their definitions, the volume

fractions clearly must fulfil the constraint $\sum_\alpha \theta_\alpha = 1$. The relation between porosity ϕ , aqueous and gaseous saturation s_α and its content is $\theta_\alpha = \phi s_\alpha$, where $s_l + s_g = 1$.

For each component $\kappa \in \mathcal{K}_\alpha$, the general macroscopic mass conservative equations describing the transport and reaction of aqueous and solid phase species are written as

$$\frac{\partial(\theta_\alpha c_{\alpha,\kappa})}{\partial t} + \nabla \cdot \{c_{\alpha,\kappa} \mathbf{v}_\alpha + j_{\alpha,\kappa}\} = R_{\alpha,\kappa}, \quad (1)$$

where $c_{\alpha,\kappa}$ is the mass concentration of component κ , \mathbf{v}_α is the velocity of phase α , $j_{\alpha,\kappa}$ is the diffusion term and $R_{\alpha,\kappa}$ describes the reaction.

We assume as in [36] and [37] that sum of the diffusive fluxes for all components in each phase is zero

$$\sum_{\kappa \in \mathcal{K}_\alpha} j_{\alpha,\kappa} = 0, \quad (2)$$

which ensures that the phase α moves with the phase velocity \mathbf{v}_α . In a typical immobile species transport equation (1), the advection and diffusion are zero and only the reaction term exists.

The phase velocity is related to the phase pressure p_α via the extended Darcy law

$$\mathbf{v}_\alpha = -\frac{k_{r\alpha}(s_\alpha)}{\mu_\alpha} K (\nabla p_\alpha - \rho_\alpha g),$$

where $k_{r\alpha}$ is the nonlinear relative permeability function, K is the scalar absolute permeability (in general it can be tensor, [38]), μ_α is the dynamic viscosity of the fluid and g is the gravitational acceleration.

The model (1) is completed by the macroscopic capillary pressure-saturation relationship

$$p_g - p_l = p_c(s_l). \quad (3)$$

Various static capillary pressure-saturation models by [39] or van [40] were developed based on laboratory experiments.

The Ficks' law is used together with the second model of Millington and Quirk for the dependence of the effective diffusion coefficient on phase saturation [41] and one obtains

$$j_{\alpha,\kappa} = -s_\alpha^2 \phi^{\frac{4}{3}} D_{\alpha,\kappa} \nabla c_{\alpha,\kappa},$$

where $D_{\alpha,\kappa}$ is the molecular diffusion coefficient of component κ in phase α .

2.1 Operator splitting approach

Many simulators for reactive multiphase flow see e.g. [37, 42, 43, 44] use a global implicit approach with full upwinding of convective terms. This results in a large

amount of numerical diffusion for the component transport with a subsequent overestimation of reaction. We follow [45, 46] and [47] and choose an operator splitting approach.

In a first step the system (1) is split into a transport and into a reaction part

$$\frac{\partial(\theta_\alpha c_{\alpha,\kappa})}{\partial t} + \nabla \cdot \{c_{\alpha,\kappa} \mathbf{v}_\alpha + j_{\alpha,\kappa}\} = 0, \quad (4a)$$

$$\frac{\partial(\theta_\alpha c_{\alpha,\kappa})}{\partial t} = R_{\alpha,\kappa}, \quad (4b)$$

then the transport part is split again in a phase transport and a phase composition part.

Phase transport

Summation of the transport part (4a) over all components of each phase and using assumption (2) yields a mass balance equation for each liquid phase

$$\frac{\partial(\theta_\alpha \rho_\alpha)}{\partial t} + \nabla \cdot \{\rho_\alpha \mathbf{v}_\alpha\} = 0. \quad (5)$$

The liquid mass phase density remains constant, while ρ_g may depend on phase composition. Both phases are assumed to be mobile, which is needed to model active gas transport, entrapment of gaseous species or gas production by microorganisms.

Component transport

Selecting a *reference* component $\kappa_{\alpha,0} \in \mathcal{K}_\alpha$ in each liquid phase, e.g. water in the liquid phase and air in the gas phase, it remains to solve the $|\mathcal{K}_l| + |\mathcal{K}_g| - 2$ component balance transport equations in the form

$$\frac{\partial(\theta_\alpha c_{\alpha,\kappa})}{\partial t} + \nabla \cdot \{c_{\alpha,\kappa} \mathbf{v}_\alpha + j_{\alpha,\kappa}\} = 0. \quad (6)$$

Reaction

Aqueous species are subject to local chemical interactions with the solid and gaseous phase by (4b) or are assumed to be at local equilibrium. The term $R_{\alpha,\kappa}$ includes all possible kind of reactions and it can be divided into a chemical or biological reaction part $r_{\alpha,\kappa}$, phase exchange between fluids $e_{\alpha,\kappa}$ and interaction between the liquid and solid phases $a_{\alpha,\kappa}$. Direct interaction between solid and gas phase is not considered.

2.2 Primary variables

The model (1) split into (4-6) is a mixture of partial differential equations (PDEs), ordinary differential equations (ODEs) and algebraic equations. The PDEs and ODEs can be solved using different choices of primary

variables and the remaining unknowns can be computed by solving algebraic equations.

In our applications we use the liquid phase and capillary pressures p_l, p_c and the concentrations $c_{\alpha,\kappa}$ of all but one component $\kappa \in \mathcal{K}_\alpha \setminus \{\kappa_{\alpha,0}\}$ for each fluid phase as primary variables. Concentrations in solid phase are always taken as primary variables.

Given these primary variables the remaining quantities can be computed as follows: water saturation is determined via the inverse function p_c^{-1} of (3). Because ρ_l is constant, the remaining concentration is given by the $|\mathcal{K}_l| - 1$ known concentrations.

The gas molar density ν_g is related to gas mass density by $\rho_g = \nu_g M_g$, where M_g is the average molar mass of gas mixture. Total pressure in the gas phase is related to the sum of the partial pressures (Dalton's law)

$$\sum_{\kappa \in \mathcal{K}_g} p_{g,\kappa} = p_g.$$

By means of the ideal gas law, partial pressures relate to the molar concentrations $c_{g,\kappa}^m$ of gas species

$$p_{g,\kappa} = RT c_{g,\kappa}^m$$

with R being the ideal gas law constant and T the temperature of the system as in [48]. In our applications, we assume constant temperature T across the considered domain.

2.3 Solution procedure

The numerical solution of two-phase flows (5) employs space discretization on a structured grid using a cell-centred finite volume method (CCFV) with two-point flux approximation and full upwinding in capillary pressure [49]. Time is discretized fully implicitly to achieve unconditional stability. The arising nonlinear equations are linearised with Newton-Method, the Jacobi matrix is derived through numerical differentiation and the resulting linear system is solved with BiCGStab iterative solver with an algebraic multigrid preconditioner [50].

To solve the solute transport (6) in advection dominated cases, the CCFV method using second order Godunov reconstruction of upwind fluxes (*minmod* slope limiter) [51, 52] together with the explicit Euler scheme in time is used. This scheme for advective transport gives accurate solution and reduces numerical diffusion. For the solution of (6) in diffusion dominated cases (mainly transport of gaseous species), we combine the CCFV method with central differencing scheme and implicit Euler time step discretization.

The system of ODEs (4b) was solved element wise using embedded Runge-Kutta-Fehlberg 4(5) method [53]

which allows automatically determined adaptive step size to reduce numerical error.

All the numerical methods were implemented and the numerical simulations were performed in the DUNE simulation framework [54, 55, 56]. The numerical code is parallelized using domain decomposition and can be applied to simulate two- and three-dimensional systems containing relatively high number of degree of freedoms.

A sequential non-iterative approach (SNIA) similar to [46] was used. After solution of the flow equations (5), the fluid velocities and phase saturations are used for component transport simulation. The transport model (6) including advection and diffusion is solved on a component basis. The resulting cell concentrations obtained from the transport are substituted into the chemical reaction model (4b). In many studies on reactive flow, a sequential iteration approach (SIA) was used, e.g. [57, 58]. For sufficiently small Courant-Friedrichs-Lewy number (CFL) the difference between SNIA and SIA is generally small (especially involving reactions with slow kinetic rates) and an operator splitting error is reduced significantly [59]. Because the explicit time discretization for component transport is used, the CFL condition is a necessary condition for stability and the transport time step in applications is restricted to fulfil $CFL = 0.4$.

If the advection of all fluid components is negligible (diffusive processes dominate advection) or if the flow is stationary and there are no large concentration gradients in the domain, the system of transport and reaction equations (4) can be coupled again and solved fully implicitly without operator splitting. This method is called direct substitution approach (DSA) and was discussed in e.g. [60, 61, 62].

In the overall scheme the time step for two-phase system is restricted only with convergence of Newton-Method (arising system is highly nonlinear) and may be larger than the time step for the transport equation. Then several steps for the component transport/reaction system are applied with one two-phase time step. If DSA approach is used, the time step size is dependent on the convergence of non-linear solver [63].

To reduce operator splitting error between phase transport and component transport, the maximal change in a cell saturation in one time step is limited to 0.1.

3 Microbial processes and model development

Aside from hydrogeological and physical conditions, bacterial transport and growth in the subsurface is influenced by many processes [8]. The nature of these processes represents a challenge for reactive transport

modelling in that one biological mechanism is often dependent on and/or influenced by another mechanism. Thus, it may be necessary to consider the interdependency of the various processes, which are relevant for microbiological growth in unsaturated and saturated porous media under steady-state and transient conditions.

We will introduce basic models based on a macroscopic approach for modelling the transport of microorganisms in saturated and unsaturated porous media, which were motivated, guided and optimised based on laboratory batch and flow-through experiments and measured data for *E. coli*, strain HB101 K12 pGLO.

3.1 Modelling attachment processes in porous media

In many laboratory and field studies, models based on a colloid filtration theory (CFT) have been used extensively to evaluate microbial transport and adhesion in saturated and unsaturated porous media, e.g. [8, 3].

Assuming that the attachment of *E. coli* cells to sand grains is reversible, the general formulation of the adhesion term $a_{l,X}$ describing cell adhesion from liquid phase is written as [24]

$$a_{l,X} = -\theta_l k_{att} \psi c_{l,X} + \theta_s k_{det} c_{s,X}, \quad (7)$$

where $c_{l,X}$ is the *E. coli* concentration in the liquid phase, $c_{s,X}$ is the *E. coli* concentration in the solid phase, k_{att} is the first-order deposition coefficient, k_{det} is the first-order detachment coefficient and ψ is a dimensionless deposition function. The solid phase mass balance equation for *E. coli* is given as

$$\frac{\partial (\theta_s c_{s,X})}{\partial t} = -a_{l,X}. \quad (8)$$

To account for time dependent deposition behaviour and decreases in the solid surface area available for bacterial adhesion, a general form for ψ is utilised as [25]

$$\psi = \left(1 - \frac{c_{s,X}}{s_l c_{s,X}^{max}} \right), \quad (9)$$

where $c_{s,X}^{max}$ is the maximum attainable bacterial concentration on the solid surface. The solid-liquid interstitial available for cell attachment decreases with water content. As $c_{s,X}$ rises, the bacteria render the solid surface less attractive for further attachment and the deposition function (9) will decrease to zero. The maximum concentration of $c_{s,X}$ will be equal to $s_l c_{s,X}^{max}$.

3.2 Modelling microbial growth kinetics

Different batch-culture experiments under varying conditions showed [64], that the kinetics of anaerobic and aerobic growth of *E. coli* is limited by the availability of

dissolved oxygen c_{l,O_2} and bioconvertible dissolved organic carbon (DOC), denoted by $c_{l,S}$. It was observed, that anaerobic growth takes place only if the amount of available oxygen is very low. If enough oxygen is available only aerobic respiration is active and the growth of *E. coli* is faster.

Furthermore, experiments with different oxygen concentrations showed the dependency of biomass production on oxygen availability. With decreasing oxygen concentration the total biomass production also declined. For constant air oxygen concentration 1-4%, the DOC was depleted even slower than in the anaerobic case. It can be explained by switching between aerobic respiration and anaerobic fermentation, which may take an additional time.

Because the cells attached to the sand grains are in direct contact with the liquid phase, we can define a *total* liquid *E. coli* concentration as $c_X = c_{l,X} + c_{s,X}\theta_s/\theta_l$. We assume, that cells in both phases are able to consume nutrients and to starve, but new cells become immediately mobile in the liquid phase and are able to attach only through attachment processes. This assumption is motivated by results of flow-through experiments with continuous DOC supply, where the measured cell concentration in the outflow was high (more than $1.0 \cdot 10^8$ cells ml^{-1} water) and the typical assumption for subsurface porous media that the majority of cells are attached to the solid is not valid.

The anaerobic and aerobic specific growth rates based on the Contois model [65] can be expressed as

$$\mu_a = \mu_{max,a} \frac{c_{l,S}}{c_X B_{S,a} + c_{l,S}} \frac{c_{l,O_2}}{c_X B_{O_2} + c_{l,O_2}}, \quad (10a)$$

$$\mu_{an} = \max\left(\mu_{max,an} \frac{c_{l,S}}{c_X B_{S,an} + c_{l,S}} - \mu_a, 0\right), \quad (10b)$$

where $\mu_{max,a}$ and $\mu_{max,an}$ are aerobic and anaerobic specific growth rates, respectively. The constants $B_{S,a}$, $B_{S,an}$ and B_{O_2} multiplied by c_X correspond to the half-saturation constants in a well known Monod kinetics [66]. The Contois modification is able to overcome better the difficulty described in [67], where the authors mentioned that the half-saturation constant in Monod model could vary even during a single growth cycle. To simulate bacterial growth in subsurface under different growth conditions, a single set of parameters, which is able to describe all possible states, is needed.

If the dissolved oxygen concentration is low, the cells are only growing anaerobically. With increasing oxygen concentration, they are growing in both modes but not faster than in situation when sufficient dissolved oxygen is available.

The reaction terms denoting growth and decay (with a rate constant d_c) of cells in the liquid and solid phase

are given by

$$r_{l,X} = \theta_l ((\mu_a + \mu_{an}) c_X - d_c c_{l,X}), \quad (11a)$$

$$r_{l,S} = -\theta_s d_c c_{s,X}. \quad (11b)$$

The balance equation for the consumable substrate and dissolved oxygen have the form

$$r_{l,S} = -\theta_l \left(\frac{\mu_a}{Y_{S,a}} + \frac{\mu_{an}}{Y_{S,an}} \right) c_X, \quad (12a)$$

$$r_{l,O_2} = -\theta_l \left(\frac{\mu_a}{Y_{O_2}} + m_o c_{l,O_2} \right) c_X, \quad (12b)$$

where the yield coefficients $Y_{S,a}$, $Y_{S,an}$ and Y_{O_2} are the links between growth and substrate utilisation and m_o is the non-growth-associated maintenance factor for oxygen. The maintenance rate is also dependent on oxygen availability.

3.3 Phase exchange in porous media

Even for the growth experiments in batch-culture with continuous shaking and instantaneous oxygen supply the measurements showed a lower oxygen content in the liquid phase that in equilibrium with the gas phase. The consumption of oxygen in water thus was faster than oxygen dissolution in air and the local equilibrium can not be assumed.

To specify macro-scale closure relationships for the mass exchange of oxygen in porous media between the gas and the water phase, we follow the model discussed in [68] and [69] based on the stagnant film model for spherical gas bubbles. The interphase mass flux is proportional to the concentration deficit in the water phase [70] and can be described by

$$-e_{g,O_2} = e_{l,O_2} = \beta a_{gw} \left(c_{l,O_2}^* - c_{l,O_2} \right), \quad (13)$$

where β is the mass exchange coefficient, a_{gw} is the effective gas-water interface and c_{l,O_2}^* is the equilibrium oxygen concentration in the liquid phase. For gases with a low solubility, like oxygen in water, the local equilibrium concentration of oxygen in water c_{l,O_2}^* can be described by a Henry's law

$$c_{l,O_2}^* = k_H^{cc} c_{g,O_2}$$

with constant k_H^{cc} and oxygen concentration in air c_{g,O_2} , see [71].

3.3.1 Mass exchange coefficient

The mass exchange coefficient β for a spherical structure with the harmonic mean particle diameter p_d is given by [72]

$$\beta = D_{l,O_2} \left(\frac{2}{p_d} + \frac{1}{\delta} \right), \quad (14)$$

where D_{l,O_2} is the oxygen diffusion coefficient in water and δ is the thickness of the stagnant film layer.

For advection flow regimes, the boundary layer thickness depends on the interface velocity. The difference between flow and interface velocity directly at the interface is in most cases very small and therefore neglected [73]. In this case, the thickness of the film layer can be expressed by

$$\delta = \sqrt{\frac{\pi p_d D_{l,O_2}}{\|\mathbf{v}_1\|}}.$$

Comparison of different mass exchange coefficient-velocity correlations for oxygen can be found in [68].

The gas-liquid interface plays a crucial role in the phase exchange in unsaturated porous media. Many relationships used to predict gas-liquid specific interfacial area, derived either from pore-scale network models, from Lattice-Boltzman simulations or from experiments can be found in literature, see e.g. [74, 75, 76, 77, 78, 79, 80].

A basic model - based on geometrical relationships - to estimate the total surface area for any packing of spheres was presented by [81]. The total effective interstitial surface area is given by

$$a_{gw} = \kappa s_g \frac{6\phi}{p_d}, \quad (15)$$

where κ is the fraction of air bubble surface area exposed to mobile water [68].

The gas-liquid interface in (15) is proportional to the gas content. However, the pore network models [82, 83] and experiments with glass beads [84, 80] proved this relationship only for $s_l > 0.3$ and the model (15) may overestimate the gas-liquid interface and thus phase exchange in regions with low water saturation.

The model (13) together with mass exchange coefficient (14) and interstitial surface area (15) describes a first-order kinetic, where the exchange rate depends on water content and only one free parameter p_d . The sensitivity of the model regarding to p_d is discussed in numerical results.

4 Laboratory experiments and numerical simulations in porous media

4.1 Porous medium

In experiments to quantify growth and attachment of *E. coli*, quartz sand (diameter: 0.2 – 0.6 mm, porosity 0.39) was used as a model porous medium. A multistep outflow experiment (MSO) was performed to investigate the flow-rate dependence of unsaturated hydraulic properties of the sand and hydraulic conductivity together with parameters for the van Genuchten model were estimated, see Table 1.

Table 1: Hydraulic parameters

van Genuchten model	
n	5.48
α	$1.21 \cdot 10^{-3} \text{ Pa}^{-1}$
porosity ϕ	0.39
permeability K	$2.6 \cdot 10^{-11} \text{ m}^2$

4.2 Adhesion parameters

In the work by [85] many flow through experiments were conducted to investigate adhesion kinetics of different *E. coli* strains. The adhesive rates for different strains may differ by many orders of magnitude (10^{-2} - 10^{-7} s^{-1}) and the adhesive kinetic needs to be established for every strain separately. For this reason we conducted similar flow through experiments to estimate the parameters in model (7) for strain HB101 K12 pGLO. The flow through experiments were conducted in stainless steel capillaries (diameter 0.4 cm, length 10 cm, filled with quartz sand) at initial bacterial concentrations ranging from $0.7 \cdot 10^8$ to $1.0 \cdot 10^9$ highly active cells ml^{-1} and pore velocities between 1.3 and 4.0 m d^{-1} . The number of cells remaining in 0.9% NaCl suspension was counted in the outflow, and flow through curves were determined.

The resulting data were then used for parameter estimation. The inverse modelling was done with a computer model which uses the Levenberg-Marquardt-Algorithm for the parameter estimation with sensitivities derived by numerical differentiation. The forward model solves the transport equation for *E. coli* concentration in water (6) together with adhesion kinetic models (7) and (8) with given initial concentrations. To eliminate numerical discretization errors in solving forward problem, a one-dimensional domain was divided into 512 elements for CCFV simulation. In each time step the concentration in the last element was taken as outflow concentration. The attachment coefficients in [24] have values between $7.7 \cdot 10^{-3}$ and $1.3 \cdot 10^{-4} \text{ s}^{-1}$, which is in a good agreement with our estimated attachment coefficient $k_{att} = 3.0 \cdot 10^{-4} \text{ s}^{-1}$. The detachment coefficient $k_{det} = 6.2 \cdot 10^{-6} \text{ s}^{-1}$ is also comparable with values $1.7 \cdot 10^{-8}$ - $3.3 \cdot 10^{-6} \text{ s}^{-1}$ reported in [24] with pore velocity about 4 m d^{-1} . The estimated maximum attainable concentration $c_{s,X}^{max}$ was $1.6 \cdot 10^8$ cells ml^{-1} porous medium. [25] measured the value of approx. $0.5 \cdot 10^8$ cells ml^{-1} porous medium for *Pseudomonas putida*.

A comparison between measured flow through curves and the solution of the transport/adhesion problem with given initial concentrations and different pore ve-

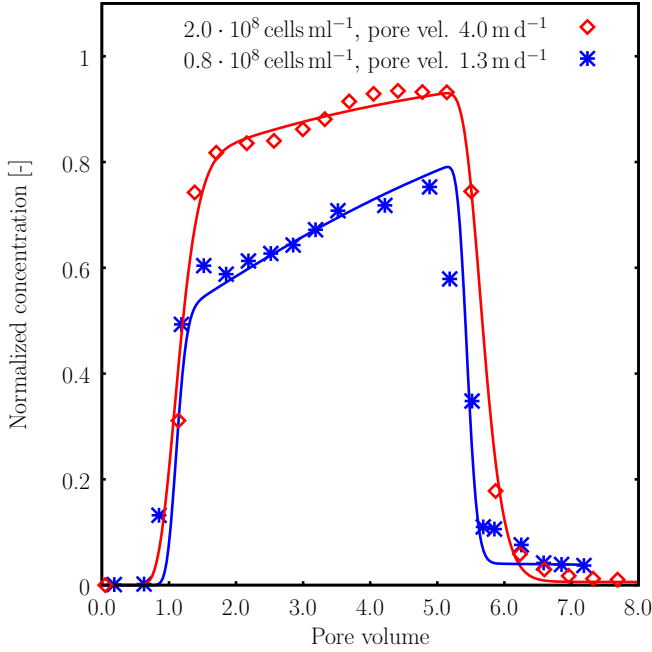


Figure 1: Flow through curves for *E. coli* HB101 K12 pGLO measured in experiments under water-saturated conditions (points) and solution of transport/adhesion problem with estimated parameters (lines).

locities is given in Fig. 1.

In the CFT the attachment rates are dependent on flow velocities, but we have not observed any dependency on flow conditions. The influence of bacterial growth stage on cell adhesion of *E. coli* has been studied by [23]. Cells in the stationary growth phase were notably more adhesive than those in the exponential phase. In our batch experiments, the age of *E. coli* cells did not have any influence on cell adhesion kinetics.

4.3 Growth parameters

Growth parameters were estimated through inverse modelling based on data from batch experiments. The estimated parameters are summarised in Table 2.

The yield coefficients of $0.95 \text{ g dryweight g}^{-1}$ consumed DOC and $0.49 \text{ g dryweight g}^{-1} \text{ O}_2$ estimated for the *E. coli* cells are in accordance with the yield coefficients reported by [86], where also $\mu_{max,a}$ values $0.39\text{--}1.39 \text{ h}^{-1}$ at high cultivation temperature of 37°C were determined. In [67] values for $\mu_{max,an}$ between 0.19 and 0.65 in Chemostat and batch cultures with glucose at $17\text{--}20^\circ\text{C}$ were listed. Under anaerobic conditions bacteria use a mixed acid fermentation (instead of respiration) to gain energy for growth [87, 88], thus the growth is slower and the yield coef-

Table 2: Growth parameters

parameter	value
$\mu_{max,a} [\text{h}^{-1}]$	0.324
$\mu_{max,an} [\text{h}^{-1}]$	0.255
$d_c [\text{h}^{-1}]$	$3.54 \cdot 10^{-3}$
$B_{S,a} [-]$	1.81
$B_{S,an} [-]$	3.07
$B_{\text{O}_2} [-]$	0.019
$Y_{S,a} [\text{g dryweight g}^{-1} \text{ consumed DOC}]$	0.95
$Y_{S,an} [\text{g dryweight g}^{-1} \text{ consumed DOC}]$	0.163
$Y_{\text{O}_2} [\text{g dryweight g}^{-1} \text{ O}_2]$	0.49
$m_o [\text{h}^{-1} \text{ g}^{-1} \text{ dryweight}]$	0.003

cient decreases. According to our results, a yield of $0.163 \text{ g dryweight g}^{-1}$ consumed DOC was determined, which is close to the anaerobic yield coefficient of $0.18 \text{ g dryweight g}^{-1}$ glucose which [89] found for some other strains of *E. coli*.

4.4 Experimental setup

To investigate growth and transport of *E. coli* under steady-state and transient conditions, a flow through chamber (FTC) with inner dimensions of $50 \times 40 \times 0.6 \text{ cm}$ filled with sand up to 30 cm was used. The whole system was kept under constant temperature $21 \pm 1^\circ\text{C}$. More detailed descriptions of the laboratory experiment can be found in [90].

At the beginning of the experiment, the porous medium was completely dry (previously heat sterilised). The suspension of *E. coli* cells and LB medium was initially injected to the chamber through six ports in the bottom of the chamber (at 5, 11.5, 21.5, 28, 39 and 44.5 cm) with a flow-rate 190 ml h^{-1} . After one hour, the water injection was stopped and the CF at the height up to 25 cm was formed, see saturation curve Fig. 2. The balance between water pressure and atmospheric pressure was at the height of 6 cm . The FTC was kept in standstill for next five days, *E. coli* cells consumed all the bioconvertible DOC and synthesised green fluorescent protein (GFP).

After five days, sterile, oxygen saturated LB medium was injected from the left side (inflow and outflow ports at height of 0.5, 2.0, 3.5 and 5.0 cm) and the same amount of liquid was extracted on the other side of the chamber by peristaltic pumps. The total flow-rate in horizontal direction was 15 ml h^{-1} and took place for next six days.

The FTC was irradiated with UV light (365 nm) and the mean fluorescence intensity, which was detected by

a camera system, was converted to cell densities, see [90]. The average dry weight m of one cell of *E. coli* was approx. $5.0 \cdot 10^{-13}$ g.

4.5 Simulation setup

Because the FTC is thin compared with the other dimensions, for numerical simulations it can be simplified as a two-dimensional domain 50×30 cm. The domain was spatially discretized using 392×256 rectangular grid cells for CCFV method, where the size of each element 1.3×1.2 mm corresponds to the twofold diameter of maximal grain size. This grid resolution is fine enough to eliminate numerical error in spatial discretization, but the runtime of numerical simulation is still acceptable.

In p_c - p_l -formulation of two-phase problem (5), an initial positive water saturation is necessary (for $s_l = 0$ is p_c infinite). To obey this restriction, initial values of p_c and p_l corresponds to 0.1% of water content and atmospheric gas pressure.

All domain boundaries excluding inlet/outlet ports are impermeable for the liquid phase (zero Neumann boundary condition). The flux in ports is identical to the experimental setup. For the gas phase all but the top side is impermeable. The air pressure at the top of the domain is fixed to the atmospheric pressure which is consistent to free boundary.

The initial amount of water is free of DOC and *E. coli* cells. The relative initial and boundary oxygen concentration in air is 20.95%. The ideal gas law yields absolute oxygen concentration of 8.68 mmol l^{-1} gas. At 21°C the Henry's constant k_H^{cc} is $3.28 \cdot 10^{-2}$ [91] and the equilibrium oxygen concentration c_{l,O_2}^* is 9.1 mg l^{-1} water.

The injected suspensions contain LB medium with 0.8 g l^{-1} of consumable DOC. At the beginning of the experiment (inflow phase), it additionally contains a negligible amount of dissolved oxygen (0.1 mg l^{-1}) and $2 \cdot 10^7 \text{ cells ml}^{-1}$ water that is equivalent to a biomass concentration of $1.0 \cdot 10^{-2} \text{ mg ml}^{-1}$. In the second part of the experiment the injected water does not contain *E. coli* cells and dissolved oxygen concentration corresponds to the equilibrium oxygen concentration c_{l,O_2}^* .

For numerical simulations we assume, that *E. coli* cells are not able to move without water flow (no molecular diffusion, $D_{l,X} = 0 \text{ m}^2 \text{ s}^{-1}$). Other diffusion coefficients were taken from literature: $D_{l,S} = 1.9 \cdot 10^{-10} \text{ m}^2 \text{ s}^{-1}$ given by [92], $D_{l,O_2} = 2.2 \cdot 10^{-9} \text{ m}^2 \text{ s}^{-1}$ and $D_{g,O_2} = 1.8 \cdot 10^{-5} \text{ m}^2 \text{ s}^{-1}$ as listed in [93].

4.6 Numerical simulation

The numerical simulation was performed as described above. Our interest is to have spatial and temporal distribution of investigated species, primarily total cell concentration $X_t = c_X \theta_l / m$ [cells ml^{-1} CF volume], mobile cell concentration $X_l = c_{l,X} \theta_l / m$ [cells ml^{-1} CF volume], oxygen and DOC concentrations in order to understand the behaviour of flow and transport of *E. coli* during the experiment. The CF volume denotes the total volume occupied by the porous medium including the pore space.

Inflow and stagnancy

The infiltration phase was stopped after 1 h, but the complete CF was established slower. After approx. 6 h no changes in saturation distribution in both, in model as well as in experiment were observed.

The concentration distributions in horizontal direction are roughly symmetrical. The simulated cell densities on a vertical cut of the two-dimensional domain at $x = 25$ cm after 5 d for $p_d = 0.9$ mm are in Fig. 2.

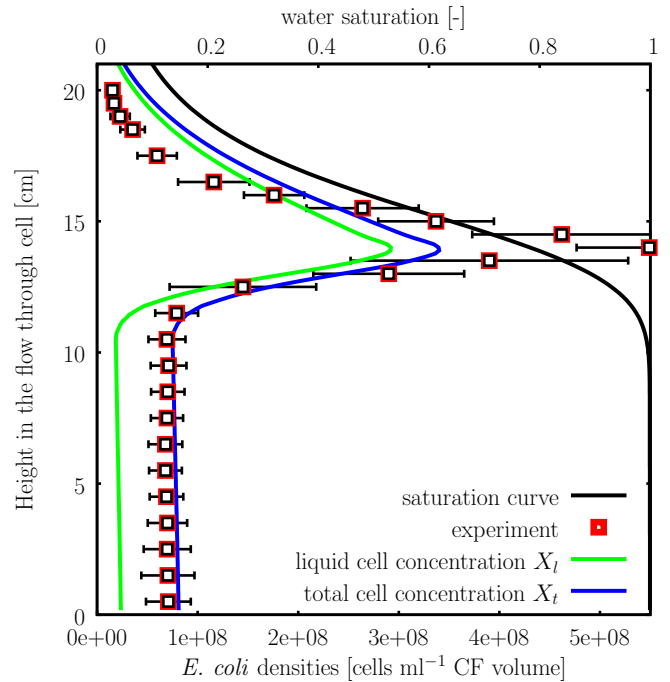


Figure 2: Vertical cut of the domain at $x = 25$ cm after 5 d of growth without new nutrient supply and without flow. Comparison between cell densities computed by numerical simulation with $p_d = 0.9$ mm and experimental data.

The lower part of the domain is up to 11 cm almost fully water saturated. In this region the *E. coli*

cells were growing without oxygen supply anaerobically and the measured *E. coli* concentration is $0.7 \cdot 10^8$ cells ml⁻¹ CFvolume. Because the attachment does not depend on flow velocity and the time in stagnancy state is long, the concentration of attached cells corresponds in the whole domain is equal to $s_{l,c_s,X}^{max}$.

Starting at the height of 11 cm, cells are growing under anaerobic as well as aerobic conditions, because oxygen diffuses from the air phase to liquid phase. The best growth activity and biomass production was observed in the zone between 12 and 16 cm, where the water saturation is 0.6 – 0.8. In this region, the cells could optimally use the bioconvertible DOC, which was initially transported into the CF by infiltration and by capillary forces, and the available dissolved oxygen.

The maximal cell density in laboratory experiment was higher than in numerical simulation ($5.3 \cdot 10^8$ compared to $3.6 \cdot 10^8$ cells ml⁻¹ CFvolume), but the uncertainty in computing cell densities from their fluorescence intensities (FI) can be significant especially for high FI intensities and the measured value is rather unrealistic. If we take water saturation into account, the maximal cell concentration in water at 14 cm is almost 11 times higher compared to the values in saturated region. Unfortunately, the yield coefficients for aerobic growth measured in batch experiments are only 6 times so height to that for anaerobic growth.

In the upper part of the domain, the simulated cell densities are proportional to the water saturation. The higher concentration than experimental data can be caused by overestimation of oxygen phase exchange or by a slightly different shape of the saturation curve in simulation and in laboratory experiment for lower water saturation.

The simulated cell densities for different values of p_d , and thus for different phase exchange rates, are compared in Fig. 3. The significant difference was observed in regions with water saturation between 0.4 and 0.95. For lower value of p_d , which corresponds to the size of the bigger grains in the sand used, the phase exchange is faster in regions with lower water saturation and model overpredicts the measured cell densities. For large values of p_d the maximal cell densities decrease and the maximum is moved upwards in the domain. In following numerical experiments, the value of 0.9 mm for parameter p_d was taken.

Horizontal flow

After 5 d in standstill, 15 ml h⁻¹ of new oxygen saturated LB medium was injected to the domain. In numerical simulations, tiny change of water saturation was observed. On the inflow side of the domain, water saturation profile rose by 4 mm and it decreased by the same value on the outflow side of the chamber.

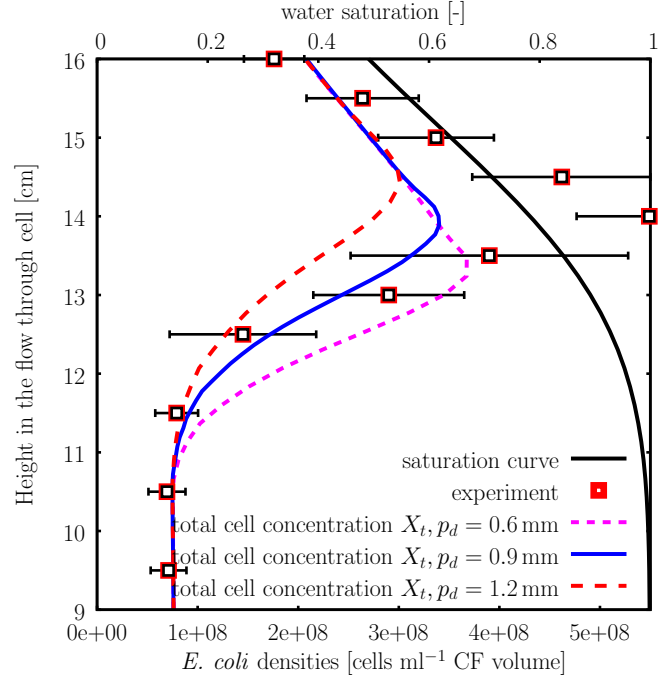


Figure 3: Vertical cut of the domain at $x = 25$ cm after 5 d of growth without new nutrient supply and without flow. Comparison between cell densities computed by numerical simulation with different values of p_d and experimental data.

This change in water saturation is too small to be detected in laboratory experiment. After several hours, the changes in water pore velocity were negligible and the flow field and saturation distribution become stationary.

The computed water velocity flow field after reaching steady-state flow conditions is shown in Fig. 4. In the middle part of the domain up to 11 – 12 cm, the water flow is quasi horizontal with pore velocity 1.3 m d⁻¹. In the unsaturated zone, the pore velocity is decreasing extensively with water saturation reduction.

Close to inlets/outlets ports, the pore velocity reaches the magnitude of 6.5 m d⁻¹. Flow is not only horizontal, but it follows the streamlines and new nutrients are transported to the upper part of the domain and also cells in the unsaturated region will get new DOC supply.

Attachment kinetic causes cells attachment and all surface of sand grains suitable for adhesion is filled up. New grown microorganisms and detached cells become part of liquid phase and are transported with water either to the unsaturated zone or are washed out of the domain.

The result of numerical simulation without new DOC supply, which is a pure artificial case, is demonstrated

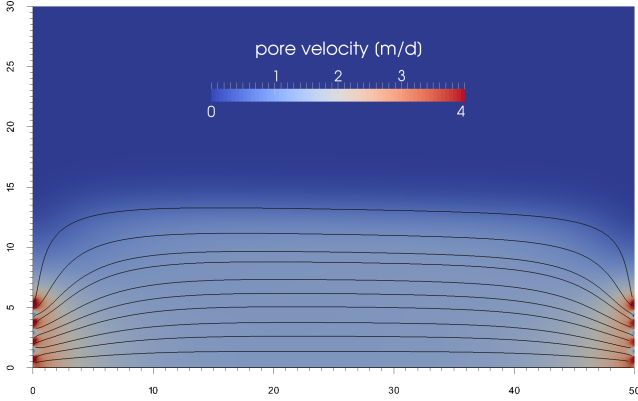


Figure 4: Magnitude of pore velocity flow field [m d^{-1}] (scaled to the maximal pore velocity 4 m d^{-1}) and streamlines of water flow.

in Fig. 5. The *E. coli* cells are highly washed away of the FTC or they are moved to the upper part of the domain, where the fluid flow is insignificant. Even the cells originally attached to the sand grains are slowly washed out, but to completely remove the attached cells in water saturated regions, it would take much longer time.

The situation with new nutrients supply is completely different. After 3 d, the transport and growth of *E. coli* become quasi-stationary and do not change considerably. The spatial distribution after 10 d (last 5 d with horizontal flow) is shown in Fig. 6.

On the inflow side of the chamber, the microorganisms are washed away and even the number of attached cells is reduced. The area with high cell concentration on the inflow side of the domain was shifted up by 2 – 3 cm.

New carbon and oxygen sources are depleted during the transport through the chamber. Oxygen in saturated and in unsaturated zone is exhausted almost immediately if the microorganism concentration is high. DOC is transported with water flow and is consumed continuously. Numerical simulation confirmed, that almost all bioconvertible DOC was consumed within transport through the chamber.

The comparison between experimental and simulated cell concentrations on a vertical cut at $x = 25 \text{ cm}$ is in Fig. 7. With numerical simulation it is possible to predict the total cell concentration well. In the upper part of the domain with very low saturation ($s_l < 0.2$) *E. coli* cells did not get any new nutrients from flowing water and were starving. The highest microbial activity is again in the transition zone between 12 and 16 cm, but the maximal cell concentration is lower than without flow (Fig. 2). The vertical flow in the saturated region causes cell attachment and the total cell concentration X_t is higher than the mobile cell concentration

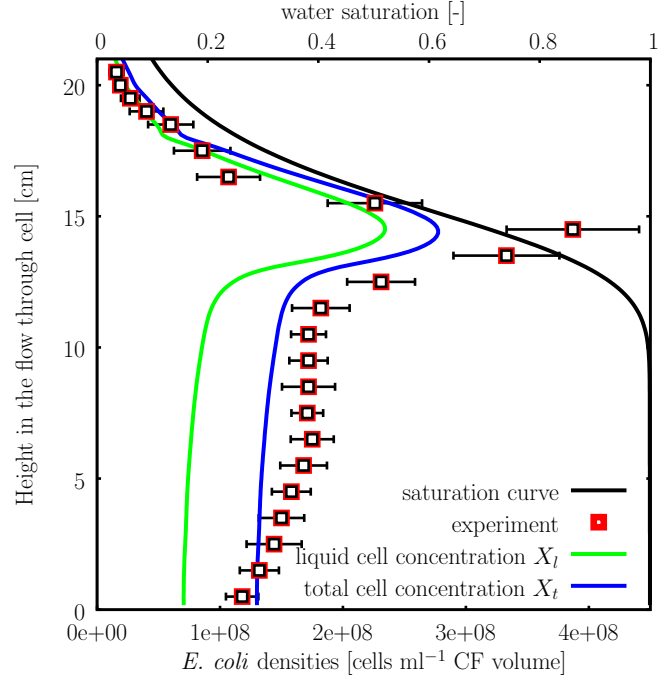


Figure 7: Vertical cut of the domain at $x = 25 \text{ cm}$ after 10 d of growth, last 5 d with new nutrient supply and horizontal flow. Comparison between cell densities computed by numerical simulation and experimental data.

X_l ; in laboratory experiment even higher cell numbers were measured.

Numerical model predicts an accumulation of *E. coli* cells in the right part of the domain above the outflow ports. From this region the cells are washed away slowly. This effect was also observed in tracer experiments with fluorescein, but not observed in the experiment with *E. coli* cells, see [94].

In addition, the production of GFP is dependent on oxygen concentration [90], but many cells were grown without oxygen supply which can limit the GFP production and in situ cell detection can be difficult in the right part of the domain. These contradiction between numerical simulation and experimental data should be taken into account and be investigate in the design of future laboratory experiments.

5 Discussion and summary

The primary objective of this study was to provide a macroscopic approach for modelling microbial growth and transport in saturated and unsaturated porous media. In pursuing this objective we have emphasised two areas of advancement. The first is development of numerical simulator for two-phase multicomponent reactive flow, and the second is model optimisation and

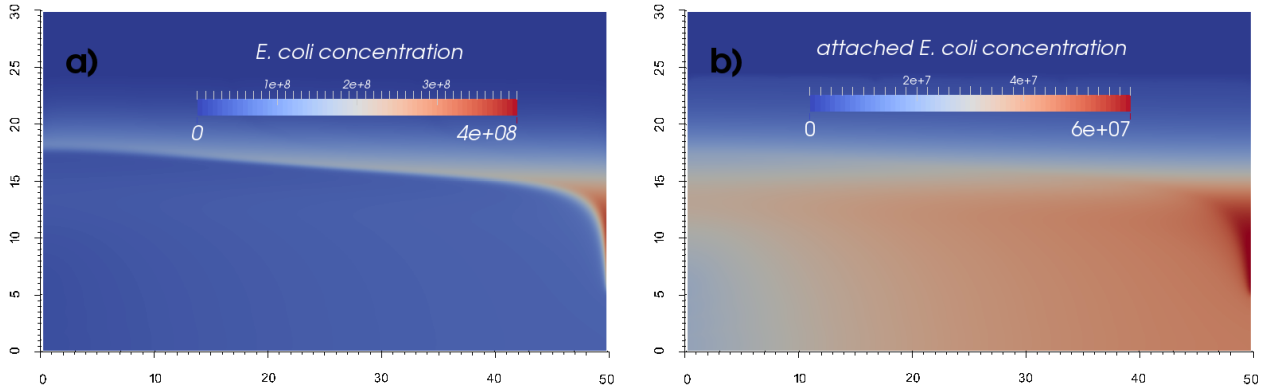


Figure 5: Situation after 10 days of simulation without new DOC supply, spatial distribution of a) total *E. coli* concentration X_t [cells ml⁻¹ CFvolume], b) attached cells [cells ml⁻¹ CFvolume].

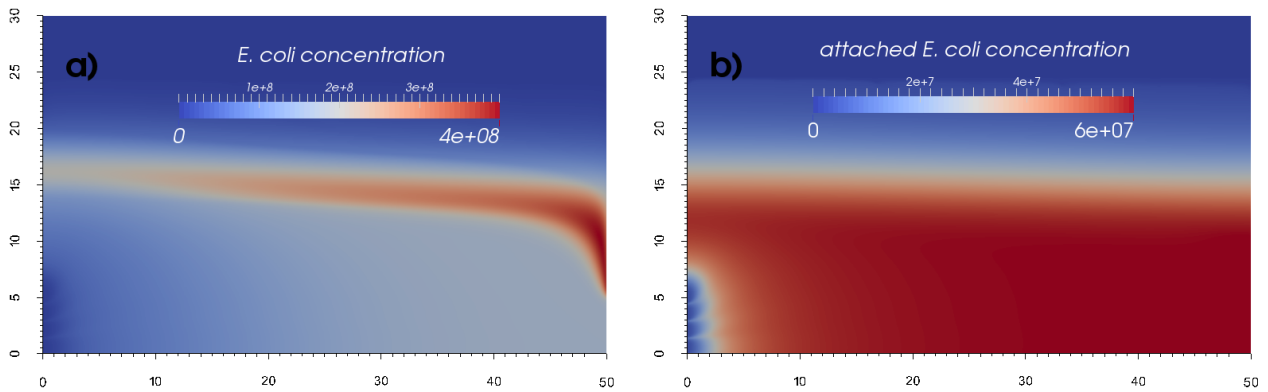


Figure 6: Situation after 10 days of simulation with new DOC supply, spatial distribution of a) total *E. coli* concentration X_t [cells ml⁻¹ CFvolume], b) attached cells [cells ml⁻¹ CFvolume].

comparison between numerical simulation and laboratory experiment data. The simulations were performed without any additional calibration of the estimated and of the used parameters.

Model formulation and numerical discretization

The model includes transient two phase movement in saturated-unsaturated porous media, multicomponent solute transport and diffusion, phase exchange, as well as a chemical model that considers chemical reactions, microbial growth and cell attachment.

The operator splitting concept allows us to use discretization schemes that are adapted in an optimal way to the individual situation dependent on flow conditions. Since reaction only takes place when components mix, the numerical diffusion in flow direction can overpredict pore-scale mixing, and thereby overpredict homogeneous chemical reaction [95].

To prevent numerical dispersion and overestimation of the reactions, higher order discretization schemes are used. Using explicit temporal discretization, the numerical diffusion in advective-dominated cases is reduced significantly, but the time step is restricted by the *CFL* condition.

If the flow is slow (diffusion dominates) or if the flow is quasi-stationary and takes place for a longer time (several pore volumes), the DSA together with implicit time discretization can be an alternative. Although the resulting system of nonlinear algebraic equations can be large, the time step is not restricted. In practise, the time step for the DSA is restricted by the convergence of Newton's method.

As the geometry of the experimental setup is rectangular, simple structured grids are sufficient. A robust, flexible, accurate, local mass conservative and efficient space discretization scheme on such grids is the CCFV. However, on complicated geometries and unstructured grids other discretization schemes like discontinuous Galerkin method can be used [96].

Microbiological growth

In order to predict microbial processes in the field or laboratory situation, we need to understand the dominate processes in the particular setting and obtain estimates of kinetic parameters.

Microbial growth and decay, cell attachment and detachment, phase exchange and transport of nutrients - these are the most important processes affecting behaviour of *E. coli* in the capillary fringe. Model describing *E. coli* growth under aerobic and anaerobic conditions and its combination based on observations in batch experiments was furthermore extended

by transport and adhesion processes. Because the advection is in our application high and a significant part of microorganisms remains in the liquid phase, we do not need to introduce a maximal microbial capacity in growth model as in [21].

By simulating *E. coli* growth and transport and subsequent consumption of DOC and oxygen, it was possible to reproduce the observed changes of biomass like in the laboratory experiment. The microbial activity was observed and modelled in the whole domain, particularly in the transition zone. In this region, the bacteria will get new DOC supply with water flow and sufficient amount of oxygen from the atmosphere.

Model limitations

In our macroscopic modelling approach, we neglected or simplified some processes which may affect growth and transport of *E. coli* and other soil microorganisms.

For adhesion kinetic we use a model based on colloid filtration theory, which is not always valid under repulsive conditions [3]. Although we assumed the same consumption kinetic in both phases, attached bacteria may consume less nutrients than cells in liquid phase. In addition, the attachment mechanism can be different in water fully saturated and unsaturated regions.

More understanding is also required on how soluble organics interact with the surfaces of bacteria and affect their retention to soil surfaces [7]. In [25, 34] the accumulation of bacteria at the air-water interface was also considered and it was modelled as an irreversible adsorption. We did not deem it necessary in this study, because no attachment and detachment from the air-water interface was observed in laboratory experiments.

We also neglected the capability of microorganisms to move in response to a chemical gradient. Both random motility and chemotaxis can have an influence to transport for subsurface organisms [8]. Motility and chemotaxis can play a role e.g. in movement of microbes into contaminated areas of low permeability, where advective transport is minimal compared with adjacent preferred flow paths [9].

The growth and transport of microorganisms can also have an influence on hydraulic properties of porous media [2]. High accumulation of microbial cells can change the hydraulic properties of porous media [97], create preferential flow paths and change flow and transport direction, which is not yet included in the model. The microbially generated gases and entrapment or microbially induced changes in the chemical properties of the liquid or solid phases of the media may also play a role in permeability reduction [98].

The models describing the formation of microcolonies and/or biofilms require microscale data that

are difficult to measure accurately [45]. Microbial colonisation may cause apparent drying within the colonised zone, with localised decreases in saturation, giving rise to partial diversion of flow around the colonised zone [2].

6 Conclusion

The developed model provides a temporally and spatially resolved quantification of microbial activity and nutrients in unsaturated and saturated porous medium. The individual submodels were optimised and calibrated based on experimental data and used for the simulation of growth and transport of *E. coli* in a flow through cell with conditions representing the capillary fringe. The results of numerical simulation can reproduce laboratory experiments very effectively. The model can be further extended and applied to optimise the design of new laboratory and field experiments.

Acknowledgements

This study was funded by DFG (German Research Foundation) through the Research Group FOR 831 “Dynamic Capillary Fringes: A Multidisciplinary Approach” (Project Ga 546/5-2 and Ba 1498/7-2).

References

- [1] Clement, T., Peyton, B.: Microbial growth and transport in porous media under denitrification conditions: experiments and simulations. *Journal of Contaminant Hydrology* **24**(3-4), 269–285 (1997). DOI 10.1016/S0169-7722(96)00014-9
- [2] Yarwood, R.R., Rockhold, M.L., Niemet, M.R., Selker, J.S., Bottomley, P.J.: Impact of microbial growth on water flow and solute transport in unsaturated porous media. *Water Resources Research* **42**(10) (2006). DOI 10.1029/2005WR004550
- [3] Tufenkji, N.: Modeling microbial transport in porous media: Traditional approaches and recent developments. *Advances in Water Resources* **30**(6-7), 1455–1469 (2007). DOI 10.1016/j.advwatres.2006.05.014
- [4] Chen, G., Walker, S.L.: Fecal indicator bacteria transport and deposition in saturated and unsaturated porous media. *Environmental Science & Technology* **46**(16), 8782–90 (2012). DOI 10.1021/es301378q
- [5] Lee, E.J., Kim, M., Kim, Y., Lee, K.K.: Numerical and field investigation of enhanced in situ denitrification in a shallow-zone well-to-well recirculation system. *Ecological Modelling* **220**(19), 2441–2449 (2009). DOI 10.1016/j.ecolmodel.2009.06.014
- [6] Bauer, R.D., Maloszewski, P., Zhang, Y., Meckenstock, R.U., Griebler, C.: Mixing-controlled biodegradation in a toluene plume—results from two-dimensional laboratory experiments. *Journal of Contaminant Hydrology* **96**(1-4), 150–68 (2008). DOI 10.1016/j.jconhyd.2007.10.008
- [7] Unc, A., Goss, M.J.: Transport of bacteria from manure and protection of water resources. *Applied Soil Ecology* **25**(1), 1–18 (2004). DOI 10.1016/j.apsoil.2003.08.007
- [8] Ginn, T.R., Wood, B.D., Nelson, K.E., Scheibe, T.D., Murphy, E.M., Clement, T.: Processes in microbial transport in the natural subsurface. *Advances in Water Resources* **25**(8-12), 1017–1042 (2002). DOI 10.1016/S0309-1708(02)00046-5
- [9] Amy, P.S., Halderman, D.L.: *Microbiology of the Terrestrial Deep Subsurface (The Microbiology of Extreme and Unusual Environments)*. CRC (1997)
- [10] Or, D., Smets, B., Wraith, J., Dechesne, A., Friedman, S.: Physical constraints affecting bacterial habitats and activity in unsaturated porous media - a review. *Advances in Water Resources* **30**(6-7), 1505–1527 (2007). DOI 10.1016/j.advwatres.2006.05.025
- [11] Sierra, J., Renault, P.: Oxygen consumption by soil microorganisms as affected by oxygen and carbon dioxide levels. *Applied Soil Ecology* **2**(3), 175–184 (1995). DOI 10.1016/0929-1393(95)00051-L
- [12] Reischke, S., Rousk, J., Bååth, E.: The effects of glucose loading rates on bacterial and fungal growth in soil. *Soil Biology and Biochemistry* **70**, 88–95 (2013). DOI 10.1016/j.soilbio.2013.12.011
- [13] Skopp, J., Jawson, M., Doran, J.: Steady-state aerobic microbial activity as a function of soil water content. *Soil Science Society of America Journal* **54**(6), 1619–25 (1990). DOI 10.2136/sssaj1990.03615995005400060018x
- [14] Chang, W., Halverson, L.: Reduced water availability influences the dynamics, development, and ultrastructural properties of *Pseudomonas putida* biofilms. *Journal of bacteriology* **185**(20), 6199–6204 (2003). DOI 10.1128/JB.185.20.6199-6204.2003
- [15] Affek, H.P., Ronen, D., Yakir, D.: Production of CO₂ in the capillary fringe of a deep phreatic aquifer. *Water Resources Research* **34**(5), 989–996 (1998). DOI 10.1029/98WR00095
- [16] Jost, D., Winter, J., Gallert, C.: Distribution of aerobic motile and non-motile bacteria within the capillary fringe of silica sand. *Water Research* **44**(4), 1279–87 (2010). DOI 10.1016/j.watres.2010.01.001
- [17] Jost, D., Winter, J., Gallert, C.: Water and Oxygen Dependence of *Pseudomonas putida* Growing in Silica Sand Capillary Fringes. *Vadose Zone Journal* **10**(2), 532 (2011). DOI 10.2136/vzj2010.0092
- [18] Kindred, J., Celia, M.: Contaminant transport and biodegradation: 2. Conceptual model and test simulations. *Water Resources Research* **25**(6), 1149–1159 (1989). DOI 10.1029/WR025i006p01149

- [19] Steefel, C., Depaolo, D., Lichtner, P.: Reactive transport modeling: An essential tool and a new research approach for the Earth sciences. *Earth and Planetary Science Letters* **240**(3-4), 539–558 (2005). DOI 10.1016/j.epsl.2005.09.017
- [20] Schäfer, D., Schäfer, W., Kinzelbach, W.: Simulation of reactive processes related to biodegradation in aquifers: 1. Structure of the three-dimensional reactive transport model. *Journal of Contaminant Hydrology* **31**(1-2), 167–186 (1998). DOI 10.1016/S0169-7722(97)00060-0
- [21] Schäfer, D., Schäfer, W., Kinzelbach, W.: Simulation of reactive processes related to biodegradation in aquifers: 2. Model application to a column study on organic carbon degradation. *Journal of Contaminant Hydrology* **31**(1-2), 187–209 (1998). DOI 10.1016/S0169-7722(97)00061-2
- [22] Kouznetsov, M.Y., Pachepsky, Y.A., Gillerman, L., Gantzer, C.J., Oron, G.: Microbial transport in soil caused by surface and subsurface drip irrigation with treated wastewater. *International Agrophysics* **18**(3), 239–247 (2004)
- [23] Walker, S.L., Redman, J., Elimelech, M.: Role of Cell Surface Lipopolysaccharides in *Escherichia coli* K12 adhesion and transport. *Langmuir* **20**(18), 7736–46 (2004). DOI 10.1021/la049511f
- [24] Bradford, S.A., Šimůnek, J., Walker, S.L.: Transport and straining of *E. coli* O157:H7 in saturated porous media. *Water Resources Research* **42**(12) (2006). DOI 10.1029/2005WR004805
- [25] Schäfer, A., Ustohal, P., Harms, H.: Transport of bacteria in unsaturated porous media. *Journal of Contaminant Hydrology* **33**(1-2), 149–169 (1998)
- [26] Powelson, D.K., Mills, A.L.: Transport of *Escherichia coli* in Sand Columns with Constant and Changing Water Contents. *Journal of Environmental Quality* **30**(1), 238–245 (2001). DOI 10.2134/jeq2001.301238x
- [27] Rockhold, M., Yarwood, R., Niemet, M., Bottomley, P., Brockman, F., Selker, J.: Visualization and modeling of the colonization dynamics of a bioluminescent bacterium in variably saturated, translucent quartz sand. *Advances in Water Resources* **30**(6-7), 1593–1607 (2007). DOI 10.1016/j.advwatres.2006.05.026
- [28] Dechesne, A., Or, D., Gülez, G., Smets, B.F.: The porous surface model, a novel experimental system for online quantitative observation of microbial processes under unsaturated conditions. *Applied and Environmental Microbiology* **74**(16), 5195–200 (2008). DOI 10.1128/AEM.00313-08
- [29] Clark, D.: The fermentation pathways of *Escherichia coli*. *FEMS Microbiology Letters* **63**(3), 223–234 (1989). DOI 10.1111/j.1574-6968.1989.tb03398.x
- [30] Madigan, M.T., Martinko, J.M., Stahl, D., Clark, D.P.: *Brock Biology of Microorganisms*, 13 edn. Benjamin Cummings (2010)
- [31] Foppen, J.W., Schijven, J.F.: Transport of *E. coli* in columns of geochemically heterogeneous sediment. *Water Research* **39**(13), 3082–8 (2005). DOI 10.1016/j.watres.2005.05.023
- [32] Lacoursiere, A., Thompson, B., Kole, M., Ward, D., Gerson, D.: Effects of carbon dioxide concentration on anaerobic fermentations of *Escherichia coli*. *Applied Microbiology and Biotechnology* **23**(5), 404–406 (1986). DOI 10.1007/BF00257042
- [33] Duffy, G., Whiting, R., Sheridan, J.: The effect of a competitive microflora, pH and temperature on the growth kinetics of *Escherichia coli* O157:H7. *Food Microbiology* **16**(3), 299–307 (1999). DOI 10.1006/fmic.1998.0242
- [34] Jiang, G., Noonan, M.J., Buchan, G.D., Smith, N.: Transport of *Escherichia coli* through variably saturated sand columns and modeling approaches. *Journal of Contaminant Hydrology* **93**(1-4), 2–20 (2007). DOI 10.1016/j.jconhyd.2007.01.010
- [35] Allen, M.: Numerical modelling of multiphase flow in porous media. *Advances in Water Resources* **8**, 162–187 (1985). DOI 10.1016/0309-1708(85)90062-4
- [36] Allen, M., Behie, G., Trangenstein, J.: *Multiphase Flow in Porous Media, Lecture Notes in Engineering*, vol. 34. Springer-Verlag (1992)
- [37] Class, H., Helmig, R., Bastian, P.: Numerical simulation of non-isothermal multiphase multicomponent processes in porous media.: 1. An efficient solution technique. *Advances in Water Resources* **25**(5), 533–550 (2002). DOI 10.1016/S0309-1708(02)00014-3
- [38] Helmig, R.: *Multiphase flow and transport processes in the subsurface*. Springer Berlin (1997)
- [39] Brooks, R., Corey, A.: Hydraulic properties of porous media. *Hydrology Paper* **3**(27) (1964)
- [40] Genuchten, M.V.: A closed-form equation for predicting the hydraulic conductivity of unsaturated soils. *Soil Science Society of America Journal* **44**, 892–8 (1980)
- [41] Jin, Y., Jury, W.: Characterizing the dependence of gas diffusion coefficient on soil properties. *Soil Science Society of America Journal* **60**(1), 66–71 (1996). DOI 10.2136/sssaj1996.03615995006000010012x
- [42] Mayer, K., Frind, E., Blowes, D.: Multicomponent reactive transport modeling in variably saturated porous media using a generalized formulation for kinetically controlled reactions. *Water Resources Research* **38**(9), 13–1–13–21 (2002). DOI 10.1029/2001WR000862
- [43] Bielinsky, A.: Numerical simulation of CO₂ sequestration in geological formations. Ph.D. thesis, Universität Stuttgart (2006)
- [44] Podgorney, R., Huang, H., Plummer, M., Gaston, D.: A globally-implicit computational framework for physics-based simulation of coupled thermal-hydro-mechanical problems: Application to sustainability of geothermal reservoirs. *Orkustofnun (National Energy Authority)* (2012)

- [45] Clement, T., Sun, Y., Hooker, B., Petersen, J.: Modeling multispecies reactive transport in ground water. *Groundwater Monitoring & Remediation* **18**(2), 79–92 (1998). DOI 10.1111/j.1745-6592.1998.tb00618.x
- [46] Xu, T., Pruess, K.: Modeling multiphase nonisothermal fluid flow and reactive transport in variably saturated fractured rocks. *American Journal of Science* **301**(1), 134–59 (2001). DOI 10.2475/ajs.301.1.34
- [47] Xu, T., Sonnenthal, E., Spycher, N., Pruess, K.: TOUGHREACT A simulation program for nonisothermal multiphase reactive geochemical transport in variably saturated geologic media: Applications to geothermal injectivity and CO₂ geological sequestration. *Computers & Geosciences* **32**, 145–165 (2006). DOI 10.1016/j.cageo.2005.06.014
- [48] Molins, S., Mayer, K.U.: Coupling between geochemical reactions and multicomponent gas and solute transport in unsaturated media: A reactive transport modeling study. *Water Resources Research* **43**(5), 1–16 (2007). DOI 10.1029/2006WR005206
- [49] Neumann, R., Bastian, P., Ippisch, O.: Modeling and simulation of two-phase two-component flow with disappearing nonwetting phase. *Computational Geosciences* **17**(1), 139–149 (2013). DOI 10.1007/s10596-012-9321-3
- [50] Blatt, M.: A Parallel Algebraic Multigrid Method for Elliptic Problems with Highly Discontinuous Coefficients. Ph.D. thesis, University of Heidelberg (2010)
- [51] LeVeque, R.J.: *Numerical Methods for Conservation Laws*. Birkhäuser Basel, Basel (1990). DOI 10.1007/978-3-0348-5116-9
- [52] LeVeque, R.J.: *Finite Volume Methods for Hyperbolic Problems*. Cambridge University Press (2002). DOI 10.1017/CBO9780511791253
- [53] Hairer, E., Nørsett, S., Wanner, G.: *Solving Ordinary Differential Equations I: Nonstiff Problems*. Solving Ordinary Differential Equations. Springer (1993)
- [54] Bastian, P., Blatt, M., Dedner, A., Engwer, C., Klöfkorn, R., Ohlberger, M., Sander, O.: A generic grid interface for parallel and adaptive scientific computing. Part I: Abstract framework. *Computing* **82**(2), 103–119 (2008). DOI 10.1007/s00607-008-0003-x
- [55] Bastian, P., Blatt, M., Dedner, A., Engwer, C., Klöfkorn, R., Kornhuber, R., Ohlberger, M., Sander, O.: A generic grid interface for parallel and adaptive scientific computing. Part II: implementation and tests in dune. *Computing* **82**(2-3), 121–138 (2008). DOI 10.1007/s00607-008-0004-9
- [56] Bastian, P., Heimann, F., Marnach, S.: Generic implementation of finite element methods in the distributed and unified numerics environment (DUNE). *Kybernetika* **46**(2), 294–315 (2010)
- [57] Yeh, G., Tripathi, V.: A critical evaluation of recent developments in hydrogeochemical transport models of reactive multichemical components. *Water Resources Research* **25**(1), 93–108 (1989). DOI 10.1029/WR025i001p00093
- [58] Šimůnek, J., Suarez, D.: Two-dimensional transport model for variably saturated porous media with major ion chemistry. *Water Resources Research* **30**(4), 115–1133 (1994). DOI 10.1029/93WR03347
- [59] Xu, T., Samper, J., Ayora, C., Manzano, M., Custodio, E.: Modeling of non-isothermal multi-component reactive transport in field scale porous media flow systems. *Journal of Hydrology* **214**(1-4), 144–164 (1999). DOI 10.1016/S0022-1694(98)00283-2
- [60] Steefel, C., Lasaga, A.: Transport of multiple chemical species and kinetic precipitation/dissolution reactions with application to reactive flow in single phase hydrothermal systems. *American Journal of Science* **294**, 529–592 (1994)
- [61] Saaltink, M., Ayora, C.: A mathematical formulation for reactive transport that eliminates mineral concentrations. *Water Resources Research* **34**(7), 1649–1656 (1998). DOI 10.1029/98WR00552
- [62] Saaltink, M., Pifarré, F., Ayora, C.: RETRASO, a code for modeling reactive transport in saturated and unsaturated porous media. *Geologica Acta* **2**(3), 235–251 (2004)
- [63] Saaltink, M.W., Carrera, J., Ayora, C.: On the behavior of approaches to simulate reactive transport. *Journal of Contaminant Hydrology* **48**(3-4), 213 – 235 (2001). DOI 10.1016/S0169-7722(00)00172-8
- [64] Hron, P., Jost, D., Gallert, C., Bastian, P., Winter, J., Ippisch, O.: Numerical simulation of growth of *Escherichia coli* in unsaturated porous media (2014). *Water Resources Research*, submitted
- [65] Contois, D.E.: Kinetics of bacterial growth: relationship between population density and specific growth rate of continuous cultures. *Journal of General Microbiology* **21**, 40–50 (1959)
- [66] Monod, J.: The growth of bacterial cultures. *Annual Reviews in Microbiology* **1**(XI) (1949)
- [67] Kovárová-Kovar, K., Egli, T.: Growth kinetics of suspended microbial cells: from single-substrate-controlled growth to mixed-substrate kinetics. *Microbiology and Molecular Biology Reviews* **62**(3), 646–666 (1998)
- [68] Geistlinger, H., Beckmann, A., Lazik, D.: Mass transfer between a multicomponent trapped gas phase and a mobile water phase: Experiment and theory. *Water Resources Research* **41**(11) (2005). DOI 10.1029/2004WR003885
- [69] Holocher, J., Peeters, F., Aeschbach-Hertig, W., Kinzelbach, W., Kipfer, R.: Kinetic Model of Gas Bubble Dissolution in Groundwater and Its Implications for the Dissolved Gas Composition. *Environmental Science & Technology* **37**(7), 1337–1343 (2003). DOI 10.1021/es025712z
- [70] Mayer, A.S., Miller, C.T.: The influence of mass transfer characteristics and porous media heterogeneity on nonaqueous phase dissolution. *Water Resources Research* **32**(6), 1551–1567 (1996). DOI 10.1029/96WR00291

- [71] Sander, R.: Modeling atmospheric chemistry: Interactions between gas-phase species and liquid cloud/aerosol particles. *Surveys in Geophysics* **20**(1), 1–31 (1999). DOI 10.1023/A:1006501706704
- [72] Clift, R., Grace, J.R., Weber, M.E.: Bubbles, drops, and particles. Academic Press Inc., New York (1978)
- [73] Niessner, J.: The role of interfacial area in two-phase flow in porous media: bridging scales and coupling models. Südwestdeutscher Verlag für Hochschulschriften (2011)
- [74] Cary, J.: Estimating the surface area of fluid phase interfaces in porous media. *Journal of Contaminant Hydrology* **15**(4), 243–248 (1994). DOI 10.1016/0169-7722(94)90029-9
- [75] Ahrenholz, B., Niessner, J., Helmig, R., Krafczyk, M.: Pore-scale determination of parameters for macroscale modeling of evaporation processes in porous media. *Water Resources Research* **47**(7) (2011). DOI 10.1029/2010WR009519
- [76] Brusseau, M., Popovicova, J., Silva, J.A.K.: Characterizing gas-water interfacial and bulk-water partitioning for gas-phase transport of organic contaminants in unsaturated porous media. *Environmental Science & Technology* **31**(6), 1645–1649 (1997). DOI 10.1021/es960475j
- [77] Chen, L., Kibbey, T.: Measurement of air-water interfacial area for multiple hysteretic drainage curves in an unsaturated fine sand. *Langmuir* **16**(22), 6874–80 (2006)
- [78] Kim, H., Rao, P.S.C., Annable, M.D.: Gaseous tracer technique for estimating air–water interfacial areas and interface mobility. *Soil Science Society of America journal* **63**, 1554–1560 (1999). DOI 10.2136/sssaj1999.6361554x
- [79] Schaefer, C.E., DiCarlo, D.A., Blunt, M.J.: Experimental measurement of air-water interfacial area during gravity drainage and secondary imbibition in porous media. *Water Resources Research* **36**(4), 885–890 (2000). DOI 10.1029/2000WR900007
- [80] Porter, M.L., Wildenschild, D., Grant, G., Gerhard, J.I.: Measurement and prediction of the relationship between capillary pressure, saturation, and interfacial area in a napl-water-glass bead system. *Water Resources Research* **46**(8) (2010). DOI 10.1029/2009WR007786
- [81] Gvirtzman, H., Roberts, P.V.: Pore scale spatial analysis of two immiscible fluids in porous media. *Water Resources Research* **27**(6), 1165–1176 (1991). DOI 10.1029/91WR00303
- [82] Reeves, P.C., Celia, M.a.: A Functional Relationship Between Capillary Pressure, Saturation, and Interfacial Area as Revealed by a Pore-Scale Network Model. *Water Resources Research* **32**(8), 2345–2358 (1996). DOI 10.1029/96WR01105
- [83] Joekar-Niasar, V., Hassanizadeh, S.M., Leijnse, A.: Insights into the Relationships Among Capillary Pressure, Saturation, Interfacial Area and Relative Permeability Using Pore-Network Modeling. *Transport in Porous Media* **74**(2), 201–219 (2007). DOI 10.1007/s11242-007-9191-7
- [84] Culligan, K.A., Wildenschild, D., Christensen, B.S.B., Gray, W.G., Rivers, M.L., Tompson, A.F.B.: Interfacial area measurements for unsaturated flow through a porous medium. *Water Resources Research* **40**(12), W12,413/1–W12,413/12 (2004). DOI 10.1029/2004WR003278
- [85] Lutterodt, G.: Transport of multiple *Escherichia coli* strains in saturated porous media. CRC Press (2012). DOI 10.1201/b11796
- [86] Reiling, H., Laurila, H., Fiechter, a.: Mass culture of *Escherichia coli*: Medium development for low and high density cultivation of *Escherichia coli* B/r in minimal and complex media. *Journal of Biotechnology* **2**(3-4), 191–206 (1985). DOI 10.1016/0168-1656(85)90038-0
- [87] Stokes, J.: Fermentation of glucose by suspensions of *Escherichia coli*. *Journal of bacteriology* pp. 147–158 (1949)
- [88] Paege, L., Gibbs, M.: Anaerobic dissimilation of glucose-C14 by *Escherichia coli*. *Journal of bacteriology* pp. 107–110 (1961)
- [89] Ataa, M., Shuler, M.: Simulation of the growth pattern of a single cell of *Escherichia coli* under anaerobic conditions. *Biotechnology and bioengineering* **XXVII**(8), 1027–1035 (1985)
- [90] Jost, D., Winter, J., Gallert, C.: Non-invasive quantification of gfp-labeled *escherichia coli* in the capillary fringe by fluorescence intensity (2014). DOI 10.2136/vzj2014.03.0028. *Vadose Zone Journal*, accepted
- [91] Dean, J., Lange, N.: Lange’s Handbook of Chemistry. No. Bd. 15 in LANGE’S HANDBOOK OF CHEMISTRY. McGraw-Hill (1999)
- [92] Hendry, M.J., Ranville, J.R., Boldt-Leppin, B.E.J., Wassenaar, L.I.: Geochemical and transport properties of dissolved organic carbon in a clay-rich aquitard. *Water Resources Research* **39**(7) (2003). DOI 10.1029/2002WR001943
- [93] Aachib, M., Mbonimpa, M., Aubertin, M.: Measurement and Prediction of the Oxygen Diffusion Coefficient in Unsaturated Media, with Applications to Soil Covers. *Water, Air, & Soil Pollution* **156**(1), 163–193 (2004). DOI 10.1023/B:WATE.0000036803.84061.e5
- [94] Jost, D., Haberer, C., Grathwohl, P., Winter, J., Gallert, C.: Oxygen transfer in a fluctuating capillary fringe: Impact of microbial respiratory activity (2014). *Vadose Zone Journal*, submitted
- [95] Gramling, C.M., Harvey, C.F., Meigs, L.C.: Reactive transport in porous media: a comparison of model prediction with laboratory visualization. *Environmental*

Science & Technology **36**(11), 2508–14 (2002). DOI 10.1021/es0157144

- [96] Bastian, P.: A fully-coupled discontinuous Galerkin method for two-phase flow in porous media with discontinuous capillary pressure. *Computational Geosciences* pp. 1–18 (2014). DOI 10.1007/s10596-014-9426-y
- [97] Taylor, S.W., Jaffé, P.R.: Biofilm growth and the related changes in the physical properties of a porous medium: 3. dispersivity and model verification. *Water Resources Research* **26**(9), 2171–2180 (1990). DOI 10.1029/WR026i009p02171
- [98] Rockhold, M., Yarwood, R., Niemet, M., Bottomley, P., Selker, J.: Considerations for modeling bacterial-induced changes in hydraulic properties of variably saturated porous media. *Advances in Water Resources* **25**(5), 477 – 495 (2002). DOI 10.1016/S0309-1708(02)00023-4